N-Doped C@Zn$_3$B$_2$O$_6$ as a Low Cost and Environmentally Friendly Anode Material for Na-Ion Batteries: High Performance and New Reaction Mechanism

Sai Wang and Xin-Bo Zhang*

Na-ion batteries (NIBs) are ideal candidates for solving the problem of large-scale energy storage, due to the worldwide sodium resource, but the efforts in exploring and synthesizing low-cost and eco-friendly anode materials with convenient technologies and low-cost raw materials are still insufficient. Herein, with the assistance of a simple calcination method and common raw materials, the environmentally friendly and nontoxic N-doped C@Zn$_3$B$_2$O$_6$ composite is directly synthesized and proved to be a potential anode material for NIBs. The composite demonstrates a high reversible charge capacity of 446.2 mAh g^{-1} and a safe and suitable average voltage of 0.69 V, together with application potential in full cells (discharge capacity of 98.4 mAh g^{-1} and long cycle performance of 300 cycles at 1000 mA g^{-1}). In addition, the sodium-ion storage mechanism of N-doped C@Zn$_3$B$_2$O$_6$ is subsequently studied through air-insulated ex situ characterizations of X-ray diffraction (XRD), X-ray photoelectron spectroscopy (XPS), and Fourier-transform infrared (FT-IR) spectroscopy, and is found to be rather different from previous reports on borate anode materials for NIBs and lithium-ion batteries. The reaction mechanism is deduced and proposed as: Zn$_3$B$_2$O$_6$ + 6Na$^+$ + 6e$^-$ $\rightleftharpoons$ 3Zn + B$_2$O$_3$ · 3Na$_2$O, which indicates that the generated boracic phase is electrochemically active and participates in the later discharge/charge progress.

The increasing natural resources scarcities, atmospheric pollution, and greenhouse effect have driven human to pay close attention to renewable energy resources and cut down on consumption of fossil fuels.[1,2] Meanwhile, Na-ion batteries (NIBs) which have potentials of large-scale electric energy storage applications are considered as excellent energy storage devices candidates for renewable energy resources due to the low cost and universal distribution of sodium sources.[3,4] The major issue in realizing NIBs application requirements lies in developing suitable electrode materials, especially low price anode materials with considerable electrochemical performance.[5] At present, in terms of economic and environmental factors, the potential anode materials for NIBs are hard carbon and low-cost

transitional metal (Mn, Fe, Cu) oxides. But some drawbacks of these materials are noticeable; for instance, the main capacity of hard carbon is exhibited at potentials that close to Na metal plating which would result in Na dendrite formation and causing safe hidden trouble.[6,7] And the drawback of MnO$_2$ lies in the low capacity which is even lower than 200 mAh g^{-1} at 50 mA g^{-1}[8]; the application of Fe$_2$O$_3$ as anodes in NIBs calls for necessary integrations with carbon materials which involves the troublesome methods or expensive instruments[9,10]; and about half the charge capacity of CuO originates from the anodic reaction at 2.3 V, indicating it is not suitable for full cells when considering available capacity and average voltage.[11,12] Therefore, efforts in exploring and synthesizing suitable anode materials with convenient technologies and low-cost raw materials are very necessary and significant.

Inorganic borates have been widely studied in the past decades due to their practical values as phosphor host materials,[13] microwave dielectric materials,[14] piezoelectricity materials,[15] flame-resistant materials, and so on.[16,17] The borates were also identified as possible candidates of anode materials in Li-ion batteries (LIBs) since 1997 and some follow-up studies researches were focused on FeBO$_3$, Cu$_3$B$_2$O$_6$, Ni$_3$B$_2$O$_6$, Co$_3$B$_2$O$_6$, but they showed much inferior electrochemical performance when compared with the corresponding metal oxides; and the lithium-ion storage mechanisms of these transition metal borates were understood to be similar to those of the corresponding metal oxides that the generated boracic phases had no electrochemistry activity.[18–20] These relatively poor lithium-ion storage abilities might be reasons that the borates were not studied in hot spot of NIBs research field in recent years when considering that the anodes of LIBs with satisfactory performance could be usually directly proved to be practicable in NIBs. Fortunately, in 2017, Fe$_3$BO$_6$@C was synthesized by calcination with the assistance of preball milling and proved to be as anode material for NIBs with reversible capacity of 514.3 mAh·g^{-1}; the sodium-ion storage mechanism was studied by ex situ X-ray diffraction (XRD) method and deduced to be the transformation reaction between Na ion and iron oxides after the initial irreversible structural evolution. Namely, the generated boracic phases were

S. Wang, Prof. X.-B. Zhang
State Key Laboratory of Rare Earth Resource Utilization
Changchun Institute of Applied Chemistry
Chinese Academy of Sciences
Changchun 130022, P. R. China
E-mail: xbzhang@ciac.ac.cn

The ORCID identification number(s) for the author(s) of this article can be found under https://doi.org/10.1002/adma.201805432

**ADVANCED
SCIENCE NEWS**
www.advancedsciencenews.com

**ADVANCED
MATERIALS**
www.advmat.de

found to be inactive which were very similar to the lithium-ion storage mechanisms of the above-mentioned transition metal borates.[21] Recently, "N-doped $Zn_3B_2O_6$" was synthesized by pyrolysis of Zn-based metal–organic framework in nitrogen and tested as anode material of NIBs, but it only delivered initial discharge/charge capacities of 327.7/96.4 mAhg⁻¹ with a Coulomb Efficiency of 30%.[22] The energy storage mechanism of "N-doped $Zn_3B_2O_6$" was not studied and is still a mystery; through the above-mentioned reported lithium and sodium-ion storage mechanisms of borates, it could be simply guessed that ZnO was formed during the initial discharge progress, but the fact that ZnO has limited reaction activity toward Na ions makes the conjecture be refused when the exhibited capacities over 280 mAh g⁻¹ in the later cycles are considered. In consideration of the low price of zinc and boron elements, the nontoxicity and environmental friendliness of ZBO together with the unknown Na ion storage mechanism, it is very meaningful and interesting to do a further detailed research on developing green and facile synthesis method toward exploring ZBO's Na ion storage abilities and mechanism.

In this manuscript, for the first time, N-doped $C@Zn_3B_2O_6$ (NC@ZBO) composite is green chemically synthesized through a pretty simple calcination method with the homogeneous mixture of boric acid, urea, and zinc acetate as reactant. When the composite is employed as anode material of NIBs in half cells, a high reversible charge capacity of 446.2 mAh g⁻¹ at 20 mA g⁻¹, safe and suitable average voltage of 0.69 V, reversible charge capacity of 376.4 mAh g⁻¹ at 100 mA g⁻¹ and retained capacity of 257.3 mAh g⁻¹ after 30 cycles are together demonstrated. What is more important is that a low-cost prototype full

cell is subsequently built with preactivated NC@ZBO as anode and $K_{0.32}Fe_{0.35}Mn_{0.65}O_2 \cdot 0.39H_2O$[23] as cathode together with cheap electrolytic solute $NaClO_4$-based electrolyte. The prototype cell could exhibit a high discharge capacity of 98.4 mAh g⁻¹ at 100 mA g⁻¹ and a considerable energy density of 185.98 Wh kg⁻¹ with an average voltage of 1.89 V. Furthermore, a high discharge capacity of 73.8 mAh g⁻¹at 1000 mA g⁻¹ could even be demonstrated and after 300 cycles a retained capacity of 43.6 mAh g⁻¹ is still delivered. The sodium-ion storage mechanism of ZBO is subsequently studied by air-insulated ex situ characterizations of XRD, X-ray photoelectron spectroscopy (XPS), FT-IR; and from the obtained result, it is found the generated boracic material enters into the electrochemical reaction with obvious appearance/disappearance phenomenon. The sodium-ion storage mechanism of ZBO is that the metallic Zn and $B_2O_3 \cdot 3Na_2O$ form during discharge progress, and when the electrode is charged to 3 V, amorphous ZBO re-forms. It is expected that these results on the NC@ZBO would draw attention of new synthesis methods and studies on the low-cost and eco-friendly borate anode materials for NIBs in the future.

Figure 1a shows the XRD patterns of the NC@ZBO and bulk ZBO, and all the diffraction peaks of the two samples can be well indexed to the 3D framework structure of ZBO which belongs to C2/c space group (ICSD code: 413 603). The crystal structure of ZBO is constructed by ZnO_4 tetrahedrons and BO_3 triangles that can offer spacious 3D Na⁺ migration diffusion channels (Figure S1, Supporting Information). FT-IR spectroscopy was further utilized to identify the presence of specific chemical groups in the as-synthesized samples in the range of 500–4000 cm⁻¹ (Figure 1b). The peaks at 3441.35, 1625.70 cm⁻¹
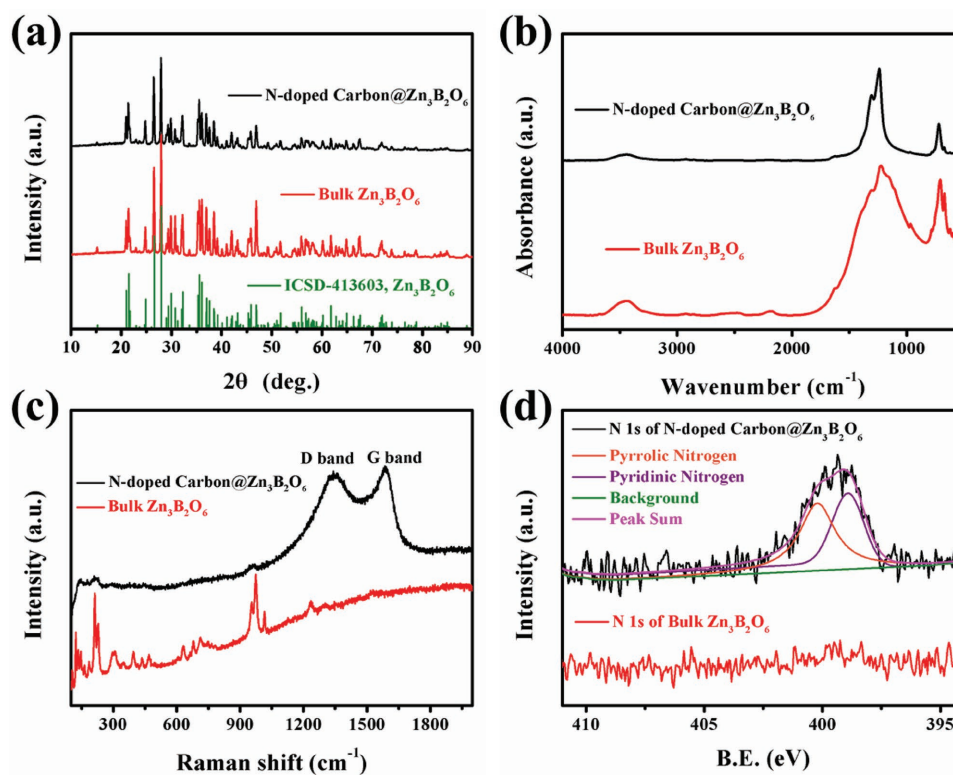

Figure 1. a) XRD patterns, b) FT-IR spectra, c) Raman spectra, and d) N 1s XPS spectra of NC@ZBO and bulk ZBO.

of NC@ZBO and 3430.74, 2476.15, 2176.28, 1622.81 cm^{-1} of bulk ZBO should be assigned to the stretching mode of −OH groups which originate from the adsorbed water.[24] The vibrations at 1305.57 and 1239.04 cm^{-1} of NC@ZBO, 1304.61 and 1223.61 cm^{-1} of bulk ZBO are originated from asymmetric stretch of B−O of triangular BO_3 group. The peaks at 719.32 cm^{-1}, (NC@ZBO) and 706.78 cm^{-1} (bulk ZBO) are derived from out-of-plane bend of B−O.[25,26] While the two peaks at 673.04 (NC@ZBO) and 670.14 cm^{-1} (bulk ZBO) are attributed to in-plane bend of B−O.[27] These analyzed FT-IR peaks are together listed in Table S1 in the Supporting Information, and similar to the XRD results, it is also hard to find great difference between the two samples from the FT-IR results. The carbon component in the NC@ZBO was confirmed through the Raman spectroscopy as shown in Figure 1c. Different from the bulk ZBO which demonstrates strong peaks between 100 and 1350 cm^{-1}, the corresponding signals of the ZBO content in the NC@ZBO are much weaker which should be related to the overlapping of the carbon. The NC@ZBO demonstrates typical and strong carbon characters with the D bond and G bond with I_D/I_G ratio of 0.98, and it is indicative of a high content of disordered type carbon in the as-synthesized materials.[28] XPS was further employed to detect N−C bonding configuration in NC@ZBO, and the presented asymmetric N 1s peak can be fitted into two peaks at 398.91 and 400.21 eV, respectively (Figure 1d). The peak at 398.91 eV is in accord with pyridinic N atoms, and the peak at 400.21 eV corresponds to

pyrrolic N atoms.[29] While for the bulk ZBO, no peak could be found. Through thermogravimetric analysis analysis, the carbon content in the NC@ZBO is calculated to be about 4.88% (Figure S2, Supporting Information).

Figure 2a,b shows the typical scanning electron microscope (SEM) images of the NC@ZBO sample. It is obviously observed that the sample consists of flake and block-shaped morphologies. The flakes and blocks pack closely and some fracture lines could be obviously found on the block-shaped morphology. The thickness of the flakes is about 10–20 nm and the sizes of the flakes and blocks are about 2–3 μm. The elemental mapping images shown in Figure 2c indicate the uniform distribution of Zn, B, O, C, and N all over the NC@ZBO composite which reveal that the flake and block-shaped all contain identical component. It is estimated that the flakes originate from fracture of the blocks that caused by the decomposing of the urea during the synthesis progress, and the agglomeration/formation of bulk block seems inevitable at a high temperature of 750 °C through such a simple method. Moreover, the bulk ZBO synthesized by ball-milling method consists of connected ZBO blocks with size in range of 3 and 10 μm that is much larger than the NC@ZBO ones (Figure S3, Supporting Information). It should be emphasized that the ZBO is found unstable under the circumstance of high electron concentration that decomposes into new phases in the transmission electron microscopy (TEM), so the TEM images of the NC@ZBO and ZBO were not taken in this article.
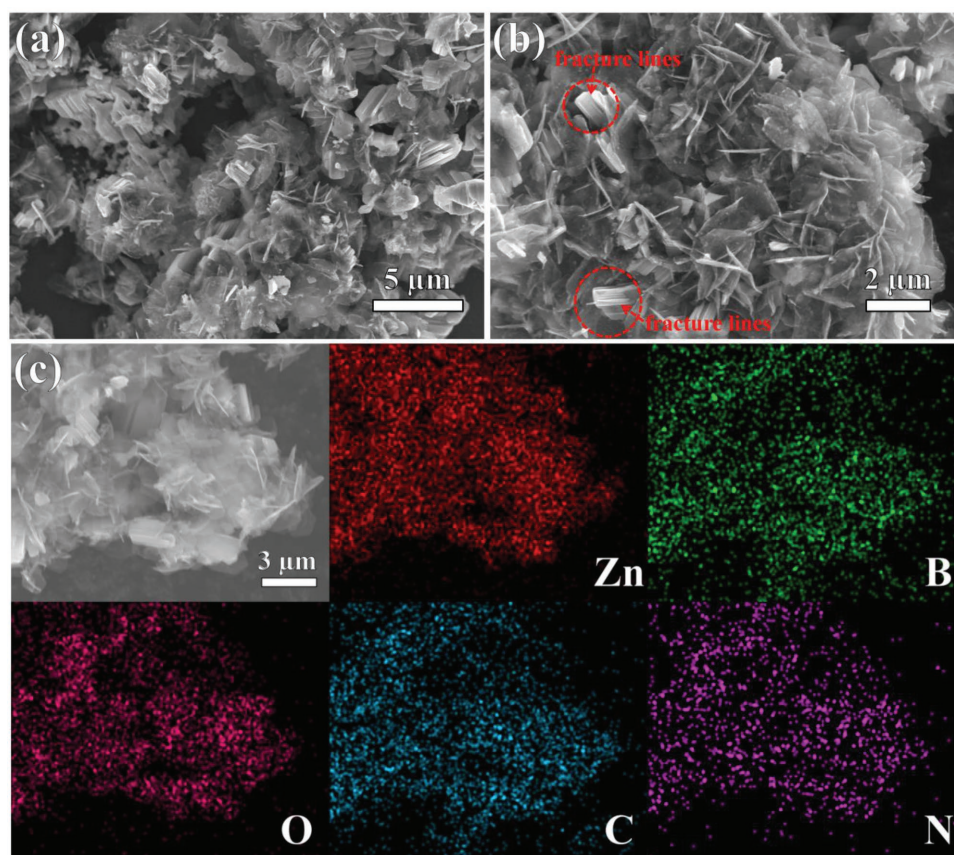

Figure 2. a,b) SEM images of NC@ZBO with different magnifications. c) Elemental mapping images of NC@ZBO.
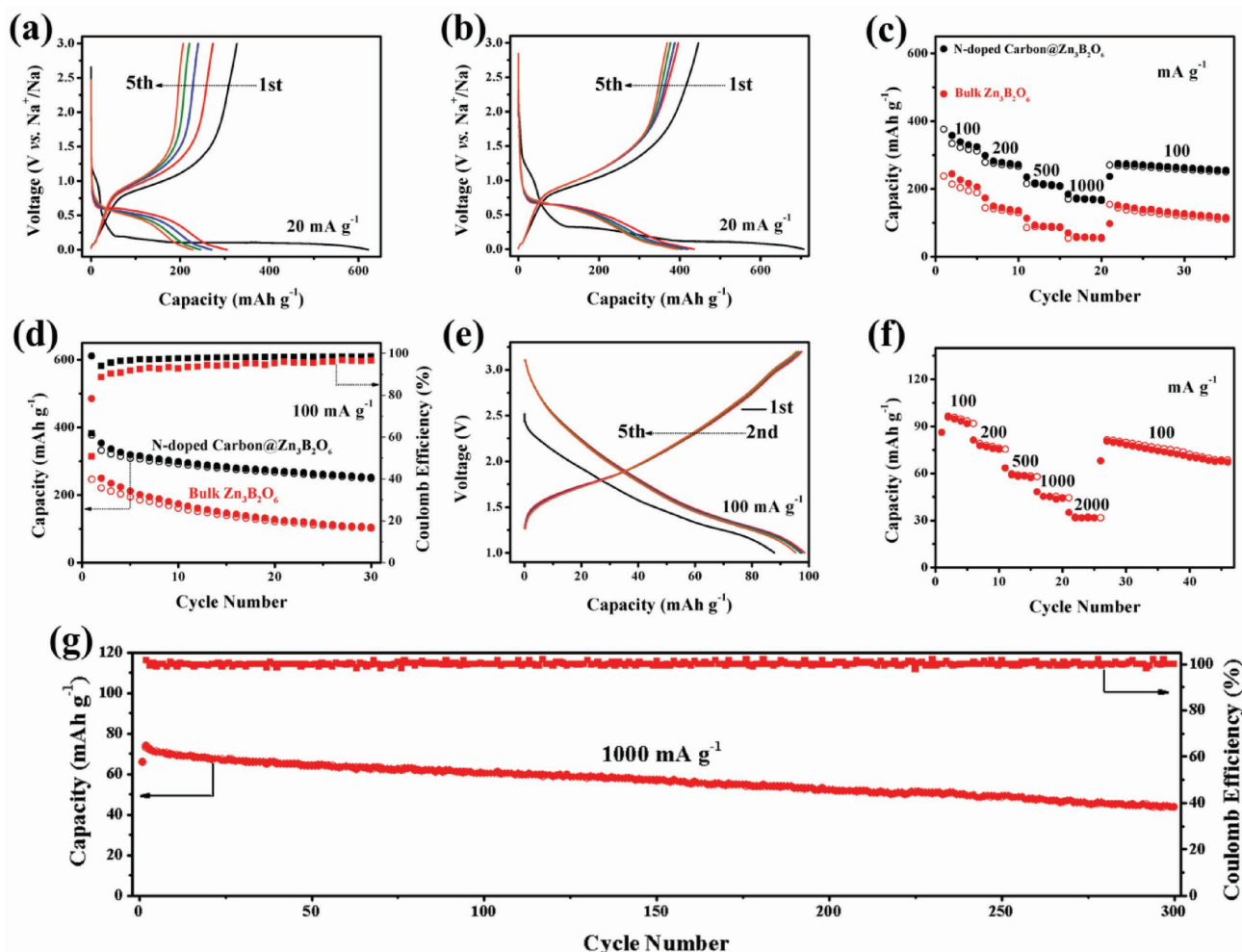
1805432 (3 of 8)

Figure 3. a,b) Discharge–charge curves of bulk ZBO and NC@ZBO, respectively (20 mA g^{-1}). c) Rate performances of bulk ZBO and NC@ZBO. d) Cycle performances of bulk ZBO and NC@ZBO (100 mA g^{-1}). e–g) Discharge–charge curves (100 mA g^{-1}), rate performance, and cycle performance (1000 mA g^{-1}) of the KFM/Na$_x$-NC@ZBO full battery, respectively.

Figure 3a exhibits the discharge–charge curves of the bulk ZBO from 1st to 5th cycle at a current density of 20 mA g^{-1} in the voltage range of 0–3 V. The pure phase material shows an initial discharge capacity of 622.3 mAh g^{-1}, and the corresponding reversible capacity is 327.2 mAh g^{-1}. Nevertheless, the capacities decay quickly and the discharge/charge capacities of the 5th cycle are only 228.3/206.7 mAh g^{-1}. It is particularly worth mentioning here that the ZnO (particle size of 20–40 nm, Figure S4, Supporting Information) shows much inferior Na ion storage ability with lower initial reversible capacity of only 66.5 mAh g^{-1} even at 20 mA g^{-1} (Figure S5a, Supporting Information); and at a relatively higher current density of 100 mA g^{-1}, the capacities stabilize around 32 mAh g^{-1} (Figure S5b, Supporting Information). From these results, it could be initially estimated that the Na ion storage mechanism of ZBO is much different from its corresponding transition metal oxide. Under the same test conditions, in a sharp contrast with bulk ZBO, the NC@ZBO demonstrates performance improvements in case of capacity values and cycle stability as shown in Figure 3b. The NC@ZBO delivers a higher initial discharge capacity of 706 mAh g^{-1} together with a charge capacity of 446.2 mAh g^{-1},

and after 5th cycle the discharge/charge capacities are 395.1/368.8 mAh g^{-1}. In case of rate performance, the bulk ZBO exhibits discharge capacities of ≈244.4, ≈149.7, ≈93.1, and ≈59.2 mAh g^{-1} at current densities of 100, 200, 500, and 1000 mA g^{-1}. While the NC@ZBO shows obvious enhanced rate abilities and displays discharge capacities of ≈357.8, ≈282.4, ≈217.4, and ≈172.8, at 100, 200, 500, and 1000 mA g^{-1}, respectively. When the current density is reset to 100 mA g^{-1}, the bulk ZBO could only show capacity of 151.6 mAh g^{-1}, but capacities over 270 mAh g^{-1} could be still obtained for the NC@ZBO (Figure 3c). The cycle performances of the two materials are further performed as shown in Figure 3d, the bulk ZBO delivers initial discharge/charge capacities of 238/480.5 mAh g^{-1} and after 30 cycles the capacities decay to 119.8/126.5 mAh g^{-1}. While for the NC@ZBO, higher initial capacities of 376.4/613.7 mAh g^{-1} and higher retained capacities of 257.3/262.5 mAh g^{-1} are exhibited. Based on the above-mentioned characterizations and electrochemistry performances, the increased sodium storage abilities of NC@ ZBO should be mainly originated from the two points: 1) The formed flake morphologies and the deceasing of the particle

size shorten the movement paths of Na ions and electrons, and could also make the N-doped C@Zn$_3$(BO$_3$) provide more active sites for electrochemical reaction. 2) The incorporation of N-doped carbon could further decrease charge-transfer resistance and this is supported by the related Nyquist plots shown in Figure S6 in the Supporting Information.

It is confirmed by the differential capacity (dQ/dV) curves that the ZBO-based materials show anodic/cathodic peaks at 0.97/0.65 V (vs Na$^+$/Na) which are away from Na metal plating potential and indicate the ZBO-based materials are suitable for full cells (Figure S7a,b, Supporting Information). So, the NC@ZBO-based Na ion full cells were fabricated later. The K$_{0.32}$Fe$_{0.35}$Mn$_{0.65}$O$_2$·0.39H$_2$O (KFM)[23] reported in our previous work was selected as cathode (the related properties of KFM-Na half cells in the same electrolyte as NC@ZBO-Na cells are in Figure S8, Supporting Information), and before assembling, the NC@ZBO anode was pre-sodiated with the purpose of reducing its irreversible capacity. The cell is cathode limited-type and the mass ratio of cathode/anode is about 0.95:1. Figure 3e illustrates the discharge-charge profiles of the full cell from the 1st to 5th cycle in the voltage range of 1 to 3.2 V at 100 mA g^{-1}. The full cell could exhibit initial discharge capacity of 87.8 mAh g^{-1} followed with the charge/discharge capacities of 97.4/98.4 to 95.6/95.4 mAh g^{-1} from the 2nd to 5th cycle. The average voltage is 1.89 V and the energy density is calculated to be 185.98 Wh kg^{-1} based on the cathode mass. The full cell also demonstrates a remarkable rate performance with discharge capacities of ≈96.4, ≈77.7 ≈59.0, ≈45.3, and ≈32.2 mAh g^{-1} at 100, 200, 500, 100, and 2000 mA g^{-1}, and high discharge capacity of 80.4 mAh g^{-1} could be still obtained when the rate comes back to 100 mA g^{-1} (Figure 3f). Inspired by the excellent rate performance of the NC@ZBO-based full cell, further cycle test at high current rate of 1000 mA g^{-1} is demonstrated as shown in Figure 3g. The NC@ZBO could still deliver high discharge capacity of 73.8 mAh g^{-1} in the second cycle and after 300 cycles the retained discharge capacity is 43.6 mAh g^{-1}. It is found that the cycle performance and the Coulomb efficiencies (≈100%) of the full cells are much better than those of the NC@ZBO-Na half cells, and this might be explained by that in the half-cell system, the side reaction between sodium mental electrode and the electrolyte could cause some degree of the capacity fading which results in an obvious negative impact on cycling. The phenomenon that the capacities of NC@ZBO-Na half cells decay quickly in the initial cycles but turn to be stable in the later cycles is mostly originated from the gradual formation of solid electrolyte interface (SEI) films on both NC@ZBO and sodium metal electrodes. In the initial cycles, the decomposition of electrolyte is very obvious. And after several cycles, stable SEI films form, the capacities turn to be stable. It should also be emphasized that from a working battery perspective, in the half cells, the NC@ZBO actually plays roles as cathode, but the sodium metal plays roles as anode. This phenomenon is not seen in the full cells in which the NC@ZBO plays real roles as anode, and the KFM plays roles as cathode. The voltage ranges of the NC@ZBO-Na half cells are also reset to be narrower (0–2 V and 0–1.5 V) than that of the KFM-NC@ZBO full cells (Figure S9, Supporting Information); but the cycle fading properties are nearly the same as the 0–3 V result (Figure 3d). This experiment date could also indicate that the cycle abilities and Coulomb

efficiencies improvements of the full cells are not originated from the narrower electrochemical window but mostly originate from the better matching between NC@ZBO anode and KFM cathode.

The air insulated ex situ XRD characterization was primarily employed to study the cycled products and understand the Na ion storage process (**Figure 4**a). It is worth stressing that the electrodes of different charge/discharge depths were prepackaged in the sample holders protected by Kapton film windows to avoid the contact with air. The electrode is first discharged to 0.25 V to detect the generated product after the cathodic peak at 0.32 V (dQ/dV curves), no new XRD peak appears and the original phase can be still found. When the electrode is further discharged to 0 V, the crystalline ZBO phase completely disappears and turns into an amorphous-like phase, and does not recover in the ends of the 2nd charge/discharge. There seems one common character peak of all the cycled patterns at ≈29.4° which might be related to the original (4 0 2) lattice plane of ZBO and this phenomenon might be caused by some unreacted ZBO with optimal orientation. It's hard to distinguish other possible phases with the standard PDF cards, and the "peaks" are so weak which might be also originated from the noisy background, so further air-insulated ex situ FT-IR characterization was taken as shown in Figure 4b. To avoid the contact with air, the progress of preparing the mixed pellets of KBr and cycled materials, together with the FT-IR test were all operated in an argon-filled glove box. The enhanced or new emerging peaks of −OH and C−H at about 3439, 2922, and 2855 cm^{-1} should be caused by the CMC binder.[30] When the NC@ZBO is first discharged to 0.25 V, the original peaks become very weak and new peaks at ≈1629 and ≈578 cm^{-1} emerge. The weak peak at ≈578 cm^{-1} (marked in gray dotted line box) should be attributed to vibrations of sodium cations through the glass network of the B$_2$O$_3$-containing glass.[31] While the strong peaks at≈1629 cm^{-1} which exist in all the cycled material should be mostly caused by SEI film formation with the bond of C=O,[32] although the −OH also shows peak near this area which might be overlapped by the SEI film. From the FT-IR and the corresponding XRD result, in the initial 0.25 V discharged state, the transform reaction has already occurred and the existence of the original XRD peaks of ZBO in this state should be related to the incomplete reaction of the ZBO. After the electrode is discharged to 0 V, the original FT-IR peaks between 1200 and 1310 cm^{-1} of the asymmetric stretch of B−O totally disappear,[25,26] new emerging boron-related peaks at 1417 (ring stretching of the boroxol groups[33]) and 1141 cm^{-1} (BO$_3$ with nonbridging oxygen[34]) are very obviously observed. Furthermore, the peaks disappearing/emerging phenomenon of the second cycle is completely consistent with the first cycle. The two weak peaks at 875 and 732 cm^{-1} marked as ① and ② in these FT-IR patterns should be attributed to CO$_3^{2-}$ of SEI film[35] and out-of-plane bend of B−O,[25,26] respectively. From the ex situ XRD and FT-IR results, it could be deduced that regular appearance/disappearance phenomenon of amorphous B$_2$O$_3$-containing glass occurs during the discharge/charge progress; this result is rather different from the previous widely held conclusions on the borate lithium-/sodium-ion storage that the generated borate phases of the initial cycle are inactive.
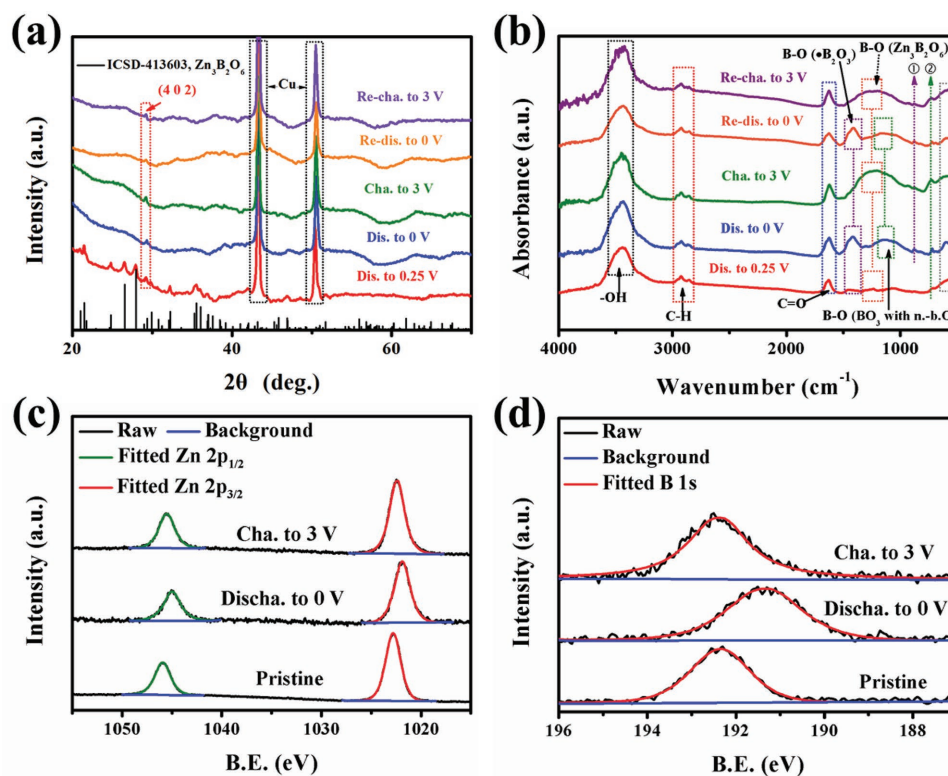
Figure 4. Air-insulated ex situ characterizations of: a) XRD, b) FT-IR, and c,d) XPS of NC@ZBO.

To further explore the reaction mechanism, air-insulated ex situ XPS characterization was taken with the assistance of a transfer device which could prevent contact with air during the electrode transfer period from the glove box to XPS instrument. It is observed that the peaks at 1022.81 (Zn 2p3/2) and 1045.92 eV (Zn 2p1/2) are close to the reported values on $ZnFe_2O_4$, indicating the oxidation state of zinc in NC@ZBO is +2.[36] After discharging, the peaks of Zn 2p3/2 and Zn 2p1/2 move to 1021.90 and 1044.98 eV, respectively, which indicates the reduction of zinc from Zn^{+2} to Zn metal.[37,38] As the electrode is charged to 3 V, the oxidation reaction happens that the Zn 2p3/2 and Zn 2p1/2 peaks come to 1022.38 and 1045.49 eV, indicating that the zinc element also participates in the discharge/charge progress and shows electrochemical activity (Figure 4c). The incomplete recovery of zinc valence might be originated from the residual sodium cations in the network of borate that share −O and lower the binding energy of Zn−O. The pristine NC@ZBO shows B 1s peak value at 192.34 eV which is close to the reported borate and indicates the valence of boron is +3.[39] After discharging, the B 1s peak turns to 191.30 eV and this peak should also relates to oxidized products (Figure 4d),[40] and the difference from that of the pristine state should be related to the BO_3 with nonbridging oxygen which is already detected in the ex situ FT-IR. The ex situ FT-IR result could explain this phenomenon as the decrease of B binding energy is related to the decrease of B−O bond which causes by the combination of O^{2-} with Na^+. Further, as the electrode is charged to 3 V, the B 1s peak nearly returns to the original state with a peak value of 192.34 eV. This XPS result shows another supporting evidence that the generated borate phase not only

participates in the electrochemical progress but also shows a high reversibility and activity. Based on the abovementioned air-insulated ex situ characterization results, it's deduced the possible and ideal reaction mechanism during the Na ion storage progress of ZBO is

$$Zn_3B_2O_6 + 6Na^+ + 6e^- \leftrightarrows 3Zn + B_2O_3 \cdot 3Na_2O \qquad (1)$$
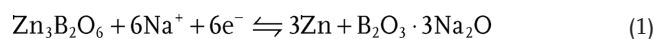
During the discharge progress, the metal zinc and $B_2O_3 \cdot 3Na_2O$ with nonbridging oxygen are generated, while during the charge progress, the amorphous ZBO re-forms. The theoretical capacity of ZBO is 512.5 mAh g⁻¹, the initial discharge capacities of bulk ZBO (622.3 mAh g⁻¹), and NC@ZBO (706 mAh g⁻¹) over this value should be attributed to the formation of SEI films that originate from the decomposition of the electrolyte.

The Li-ion storage abilities of NC@ZBO and ZnO were also tested for further illustrating the ion storage difference between ZBO and ZnO (Figure S10, Supporting Information). As anode material of LIBs, NC@ZBO could exhibit an initial discharge capacity of 941 mAh g⁻¹, and the corresponding reversible charge capacity is 615.7 mAh g⁻¹ (Figure S10a, Supporting Information). While in the case of ZnO, it delivers an initial discharge capacity of 1478.9 mAh g⁻¹ accompanied by a charge capacity of 706.4 mAh g⁻¹ (Figure S10b, Supporting Information). The capacities fading phenomena are obvious for the both two samples, and at the fifth cycle the capacities decay to 457.7/439.6 (NC@ZBO) and 504/452.7 mAh g⁻¹ (ZnO), respectively. After observing the dQ/dV curves of NC@ZBO and ZnO (Figure S10c, Supporting Information), it is estimated

that the main difference (0.6–2 V, vs Li$^+$/Li) should be related to the different types of anions in the two samples, and this result could be assisted proofs of the different ion storage mechanisms between ZBO and ZnO. The NC@ZBO could exhibit a better cycle ability than the ZnO that after 70 cycles, the discharge/charge capacities of NC@ZBO are 310.1/307.2 mAh g^{-1}, while the corresponding values of ZnO are only 185.7/184.2 mAh g^{-1} (Figure S10d, Supporting Information).

It should be emphasized that the synthesis method of NC@ZBO can also be extended to prepare other relevant borate composite, namely, cheap N-doped C@Mn$_3$B$_2$O$_6$ (NC@MBO). Except that the zinc acetate dehydrate was replaced by manganese (II) acetate tetrahydrate (manganese source) and the evaporation time was prolonged to 21 h, the other steps were all the same as those of the NC@ZBO. From the XRD result of NC@MBO (Figure S11, Supporting Information), it could be obviously found that all the peaks match well with the standard ICSD date. Theoretically, the NC@MBO could also exhibit certain Na ion storage abilities.

In summary, as a proof-of-concept experiment, NC@ZBO composite is facilely synthesized and demonstrated to be low-cost, green, and promising anode for NIBs. Compared to the pure-phase ZBO, the composite could exhibit enhanced sodium-ion storage abilities with a high reversible charge capacity of 446.2 mAh g^{-1} at 20 mA g^{-1}, safe and suitable average voltage of 0.69 V, charge capacity of 376.4 mAh g^{-1} at 100 mA g^{-1} together with retained capacity of 257.3 mAh g^{-1} after 30 cycles. A low-cost NC@ZBO-based full cell with high discharge capacity of 98.4 mAh g^{-1} at 100 mA g^{-1} and a remarkable energy density of 185.98 Wh kg^{-1} together with an average voltage of 1.89 V is subsequently built. Further, the full cell could even demonstrate a high discharge capacity of 73.8 mAh g^{-1} at 1000 mA g^{-1} with a retained capacity 43.6 mAh g^{-1} after 300 cycles. In addition, the sodium-ion storage mechanism of NC@ZBO is subsequently studied by air-insulated ex situ characterizations of XRD, XPS, and FT-IR. It is found the generated boracic material enters into the electrochemical reaction with obvious appearance/disappearance phenomenon. The possible and ideal reaction mechanism during the Na ion storage of ZBO is through this chemical equation: $Zn_3B_2O_6 + 6Na^+ + 6e^- \rightleftharpoons 3Zn + B_2O_3 \cdot 3Na_2O$. It's hoped the results presented here might encourage more researches on exploring and synthesizing low-cost and environment friendly borate anode materials with preferable sodium-ion storage abilities for NIBs in the immediate future.

Supporting Information

Supporting Information is available from the Wiley Online Library or from the author.

Acknowledgements

Conflict of Interest

The authors declare no conflict of interest.

Keywords

[1] Q. Zhang, E. Uchaker, S. L. Candelaria, G. Cao, *Chem. Soc. Rev.* **2013**, *42*, 3127.
[2] F. Cheng, J. Liang, Z. Tao, J. Chen, *Adv. Mater.* **2011**, *23*, 1695.
[3] X. Xiang, K. Zhang, J. Chen, *Adv. Mater.* **2015**, *27*, 5343.
[4] Y. Fang, X.-Y. Yu, X. W. Lou, *Adv. Mater.* **2018**, *30*, 1706668.
[5] Y. Li, Y. Lu, C. Zhao, Y.-S. Hu, M.-M. Titirici, H. Li, X. Huang, L. Chen, *Energy Storage Mater.* **2017**, *7*, 130.
[6] C. Bommier, W. Luo, W.-Y. Gao, A. Greaney, S. Ma, X. Ji, *Carbon* **2014**, *76*, 165.
[7] Z. Jian, Z. Xing, C. Bommier, Z. Li, X. Ji, *Adv. Energy Mater.* **2016**, *6*, 1501874.
[8] D. Su, H.-J. Ahn, G. Wang, *J. Mater. Chem. A* **2013**, *1*, 4845.
[9] N. Zhang, X. Han, Y. Liu, X. Hu, Q. Zhao, J. Chen, *Adv. Energy Mater.* **2015**, *5*, 1401123.
[10] Z.-J. Zhang, Y.-X. Wang, S.-L. Chou, H.-J. Li, H.-K. Liu, J.-Z. Wang, *J. Power Sources* **2015**, *280*, 107.
[11] L. Wang, K. Zhang, Z. Hu, W. Duan, F. Cheng, J. Chen, *Nano Res.* **2014**, *7*, 199.
[12] S. Yuan, X.-L. Huang, D.-L. Ma, H.-G Wang, F.-Z. Meng, X.-B. Zhang, *Adv. Mater.* **2014**, *26*, 2273.
[13] S. Verma, K. Verma, D. Kumar, B. Chaudhary, S. Som, V. Sharma, V. Kumar, H. C. Swart, *Phys. B* **2018**, *535*, 106.
[14] M. Ma, Z. Fu, Z. Liu, Y. Li, *Ceram. Int.* **2017**, *43*, S292.
[15] S. Haussühl, L. Bohatý, P. Becker, *Appl. Phys. A* **2006**, *82*, 495.
[16] Z. Zhang, W. Wu, M. Zhang, J. Qu, L. Shi, H. Qu, J. Xu, *Appl. Surf. Sci.* **2017**, *425*, 896.
[17] H. Yu, N. Z. Koocher, J. M. Rondinelli, P. S. Halasyamani, *Angew. Chem., Int. Ed.* **2018**, *57*, 6100.
[18] Y. Idota, T. Kubota, A. Matsufuji, Y. Maekawa, T. Miyasaka, *Science* **1997**, *276*, 1395.
[19] J. L. C. Rowsell, J. Gaubicher, L. F. Nazar, *J. Power Sources* **2001**, *97–98*, 254.
[20] A. Débart, B. Revel, L. Dupont, L. Montagne, J.-B. Leriche, M. Touboul, J.-M. Tarascon, *Chem. Mater.* **2003**, *15*, 3683.
[21] J. Tian, B. Wang, F. Zhao, X. Ma, Y. Liu, H. K. Liu, Z. Huang, *Chem. Commun.* **2017**, *53*, 4698.
[22] B. Yang, H. Liu, R. Lv, H. Li, X. Fu, J. Su, X. Liu, W. Gu, *Bull. Chem. Soc. Jpn.* **2018**, *91*, 548.
[23] S. Wang, Y.-H. Zhu, J.-M. Yan, X.-B. Zhang, *J. Mater. Chem. A* **2018**, *6*, 13075.
[24] C. Ramki, R. E. Vizhi, *Mater. Chem. Phys.* **2018**, *205*, 138.
[25] W. G. Zou, M. K. Lü, F. Gu, S. F. Wang, G. J. Zhou, Z. L. Xiu, H. Y. Xü, *Mater. Lett.* **2005**, *59*, 1020.
[26] M. Mousavi-Kamazani, R. Rahmatolahzadeh, S. A. Shobeiri, *J. Mater. Sci: Mater. Electron.* **2017**, *28*, 17961.
[27] Z. Wang, H. Li, G. Cai, Z. Jin, *Powder Diffr.* **2016**, *31*, 110.
[28] A. C. Ferrari, J. Robertson, *Phys. Rev. B* **2000**, *61*, 14095.
[29] S. Liu, J. Zhou, H. Song, *Adv. Energy Mater.* **2018**, *8*, 1800569.
[30] S. Mishra, G. U. Rani, G. Sen, *Carbohydr. Polym.* **2012**, *87*, 2255.
[31] V. Sharma, S. P. Singh, G. S. Mudahar, K. S. Thind, *New J. Glass Ceram.* **2012**, *2*, 150.

[32] L. Chen, K. Wang, X. Xie, J. Xie, *J. Power Sources* **2007**, *174*, 538.

[33] J. Singh, S. P. Singh, D. Singh, G. S. Mudahar, K. S. Thind, *Mater. Phys. Mech.* **2011**, *11*, 17.

[34] K. I. Cho, S. H. Lee, K. H. Cho, D. W. Shin, Y. K. Sun, *J. Power Sources* **2006**, *163*, 223.

[35] Y. Zhao, Q. Pang, Y. Meng, Y. Gao, C. Wang, B. Liu, Y. Wei, F. Du, G. Chen, *Chem. - Eur. J.* **2017**, *23*, 13150.

[36] L. Zhang, Y. Wang, Q.-Q. Ni, *Mater. Chem. Phys.* **2010**, *124*, 1029.

[37] A. Quek, R. Balasubramanian, *J. Air Waste Manage. Assoc.* **2009**, *59*, 747.

[38] V. Sirtori, F. Zambon, L. Lombardi, *J. Electron. Mater.* **2000**, *29*, 463.

[39] B. Xu, T. Li, Y. Zhang, Z. Zhang, X. Liu, J. Zhao, *Cryst. Growth Des.* **2008**, *8*, 1218.

[40] Y. J. Zou, X. W. Zhang, Y. L. Li, B. Wang, H. Yan, J. Z. Cui, L. M. Liu, D. A. Da, *J. Mater. Sci.* **2002**, *37*, 1043.